Check for updates

How to cite: *Angew. Chem. Int. Ed.* **2024**, e202414445
doi.org/10.1002/anie.202414445

Photocatalysis

Singlet Oxygen Photocatalytic Generation by Silanized TiO_2 Nanoparticles

Francesco Parrino, Alessandro Gottuso, Lorenzo Viganò, Pietro Mariani, Irene Villa, Francesca Cova, Emanuela Callone, Sandra Dirè, Leonardo Palmisano, Matus Stredansky, and Massimiliano D'Arienzo*

Abstract: A commercial TiO_2 sample, used as received or hydrothermally treated to increase surface hydroxylation, has been functionalized by surface modification with hexadecyltrimethoxysilane. The anchoring of the silane has been characterized by means of FTIR and solid-state NMR spectroscopies, and the grafting density was determined by thermogravimetric and N_2 physisorption analyses. The silane moieties induce a partial decrease of the shielding of the valence electrons of the Ti ions at the surface, and a local modification of their crystal field, as demonstrated by XPS and UV/Vis spectroscopy, respectively. The changes in coordination and the produced oxygen vacancies result in the formation of Ti^{3+} defects localized in the sub-surface region, as revealed by EPR spectroscopy. These paramagnetic centers are stabilized in the silanized samples, as the electron transfer to O_2 is efficiently inhibited even under UV irradiation. However, the amount of Ti^{3+} centers appears to be correlated with the singlet oxygen ($^1O_2$) formation rate. Accordingly, epoxidation of limonene under UV light, chosen as a model photocatalytic reaction triggered by $^1O_2$, occurred with higher selectivity when TiO_2 was silanized and upon simultaneous NIR irradiation. These evidences suggest that in the silanized sample $^1O_2$ may be generated through Förster-type energy transfer from excited sub-surface Ti^{3+} centers.

Introduction

The current industrial use of TiO_2 mainly relies upon its high refractive index and its UV-light absorbing capability.[1] In fact, TiO_2 is mainly used as white pigment for rubber and thermoplastic compounds, and as UV-light blocker for a wide range of cosmetic and personal care products. Ensuring TiO_2-matrix compatibility and filler dispersibility is essential for many of these applications, and surface silanization is one of the most used methods to achieve the above-described targets.[2]

Silanization is also carried out to suppress the photo-production of harmful reactive oxygen species (ROS) in sunscreen and cosmetic formulations. In fact, these products often contain nanostructured TiO_2 in its less photoactive rutile phase and in the "coated" form, in order to suppress *in vitro* cytotoxicity.[3] For these reasons, and because of the outstanding stability of the silyl moiety compared to other anchoring agents,[4] silanization is essentially the most used TiO_2 surface modification technique. It is therefore surprising that still fundamental questions remain open on the photo-induced behaviour of this material, in particular as far as the photo-generation of singlet oxygen, an elusive but rather powerful ROS, is concerned.

Photocatalytic degradation studies in literature could be a good starting point, even if the results are often difficult to be compared due to the variety of preparation techniques, grafting agents, reaction conditions and specific surface-substrates interactions. Moreover, most of the studies provide controversial interpretations of results because the activity of silanized TiO_2 samples is often evaluated through degradation of dyes, thus making it difficult to exclude indirect photocatalytic mechanisms or parallel photochemical processes.[5]

On the other hand, the performances of silanized TiO_2 nanoparticles (NPs) in photocatalytic partial oxidations or selective syntheses are often highly informative.[6]

[*] Prof. F. Parrino, Dr. A. Gottuso, Dr. E. Callone, Prof. S. Dirè
Department of Industrial Engineering
University of Trento
Via Sommarive 9, 38123 Trento, Italy
E-mail: francesco.parrino@unitn.it

Dr. L. Viganò, Dr. P. Mariani, Dr. I. Villa, Dr. F. Cova, Prof. M. D'Arienzo
Department of Materials Science (INSTM)
University of Milano-Bicocca
Via R. Cozzi 55, 20125 Milano, Italy

Prof. L. Palmisano
Department of Engineering
University of Palermo
Viale delle Scienze ed. 6, 90128 Palermo, Italy

Dr. M. Stredansky
Istituto Officina dei Materiali-CNR
Laboratorio TASC
Strada Statale 14, km 163.4, 34012, Trieste, Italy

© 2024 The Authors. Angewandte Chemie International Edition published by Wiley-VCH GmbH. This is an open access article under the terms of the Creative Commons Attribution License, which permits use, distribution and reproduction in any medium, provided the original work is properly cited.

© 2024 The Authors. Angewandte Chemie International Edition published by Wiley-VCH GmbH

Generally, TiO_2 silanization is applied in photocatalysis to tune the affinity of selected reactants or products with the surface of the photocatalyst.[7] In this regard, the surface tuning effect offered by silanization has been particularly beneficial for the selectivity of some partial oxidation reactions, such as the synthesis of phenol from benzene[8] and of cyclohexanone from cyclohexane.[9]

Recently, albeit indirectly, it has been proposed that TiO_2 silanization affects the selectivity of photocatalytic degradative or synthetic reactions also by influencing the primary events of the reactions.[10]

For instance, cyanuric acid could be degraded in the presence of silanized TiO_2, while it was stable in the presence of bare TiO_2.[11] Authors attributed this evidence to the fact that silanization promotes the formation of singlet oxygen, which unlike other ROS, is able to degrade the recalcitrant substrate.

Similar effect has also been invoked for the photocatalytic epoxidation of limonene to 1,2 limonene epoxide, which occurs under simulated solar irradiation with higher selectivity in the presence of silanized TiO_2 or mixed TiO_2/SiO_2 photocatalysts compared to the naked TiO_2 sample.[12,13] Analogously, it was demonstrated that the high oxygen scavenging ability displayed by hybrid organic/inorganic nanocomposites containing silanized TiO_2 relies mainly on the favoured formation of $^1O_2$ compared to the bare oxide.[14]

The preferential formation of singlet oxygen in silanized TiO_2, hypothesized indirectly to justify those activity results, suggests that silanization could influence not only the surface features, but also the primary charge or energy transfer taking place soon after the light absorption step.[15] In fact, unlike hydroxyl and superoxide radicals, singlet oxygen photogeneration does not involve a net charge transfer from molecular oxygen, and mainly relies on energy transfer driven mechanisms. Even though other mechanisms, such as the direct optical excitation of adsorbed molecular oxygen[16] or the photo-detachment of an electron from an excited superoxide radical anion[17] have been also proposed, three main energy transfer driven mechanisms can be hypothesized: (i) trivial, (ii) Dexter-like, and (iii) Förster-like.[18] As pointed out by Daimon and Nosaka,[19] trivial mechanisms triggered by radiative emission from the excited semiconductor are less probable, due to the mismatch between the emitted energy and that required to excite the triplet state. On the other hand, according to the Dexter-like mechanism, molecular oxygen could undergo a double electron transfer in opposite directions, without net charge transfer. In other words, sequentially or in a concerted way, oxygen is first reduced to superoxide, which in turn is oxidized to singlet oxygen.[20] Instead, the Förster-like mechanism does not require orbital overlapping between energy donor and acceptor, and results from long-range interactions triggered by the oscillating electric field produced locally by separated charges. This behaves as a virtual photon, exciting oxygen through a dipole–dipole interaction.[21] In this respect, Macyk et al.[22] proposed that Ti^{3+} sites, deriving from electrons populating the conduction band, could be further excited to energy states (Ti^{3+}*) localized close and within the conduction band. The excitation energy of this transition ($\lambda_{max} \approx 780$ nm) is compatible with that required to excite molecular oxygen to its singlet state. While several hypotheses are reported in bare TiO_2, to the best of our knowledge detailed studies on singlet oxygen generation onto silanized TiO_2 nanoparticles have not been reported so far. This fundamental topic is worth of being investigated in order to shine a light also on possible safety problems related to the wide use of silanized TiO_2 for cosmetic and personal care products.

Results and Discussion

TiO_2 functionalization and characterization

Scheme 1 briefly shows the functionalization with hexadecyltrimethoxy silane (HDTMS) of a commercial TiO_2 sample used as received (P25) and after a hydrothermal treatment (P25_HT) carried out to enhance the hydroxylation degree.[23] Experimental details are reported in Section S1, Supporting Information. The modified samples are labelled as P25@HD and P25_HT@HD.

The chemico-physical characterization of pristine and modified TiO_2 nanoparticles is presented in details in Section S2, Supporting Information.

ATR-FTIR analyses (Figure S1) performed on P25 and P25_HT showed that the hydrothermal treatment increased the amount of surface hydroxyl groups. The appearance in both P25@HD and P25_HT@HD spectra of vibrations due to alkyl groups of the aliphatic chain and to siloxane bonds of the condensed silaneconfirmed the effective functionalization of TiO_2 samples with HDTMS.[24–27]

Further information on the surface functionalization with HDTMS was provided by multinuclear solid-state NMR.

The ^{13}C CPMAS NMR spectrum of P25@HD (Figure S2, Panel a) points out complete hydrolysis of the alkoxysilane, due to the absence of $–OCH_3$ signals, and good degree of HDTMS condensation, based on the chemical shift of $Si–CH_2–(C1)$ resonance.[28,29] In addition, different aliphatic chain conformations[28] can be deduced from the asymmetric lineshape of the resonances of methylene groups C3–C14 (see profile fitting in Figure S3, Supporting Information). ^{29}Si CPMAS NMR spectrum (Figure S2, Panel b) is characterized by an asymmetric band due to the overlapping of T^3, T^2 and T^1 resonances (T^n represents $SiCO_3$ units, where n is

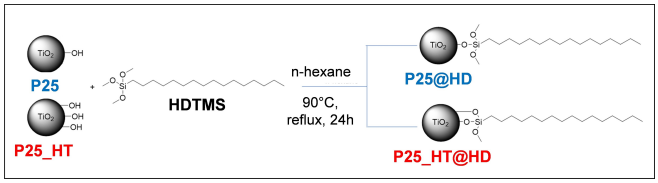

Scheme 1. Functionalization with hexadecyltrimethoxy silane (HDTMS) of TiO_2 used as received (P25) and hydrothermally treated (P25_HT). The functionalized samples are labelled as P25@HD and P25_HT@HD, respectively.

© 2024 The Authors. Angewandte Chemie International Edition published by Wiley-VCH GmbH

15213773, 0, Downloaded from https://onlinelibrary.wiley.com/doi/10.1002/anie.202414445 by CochraneItalia, Wiley Online Library on [09/11/2024]. See the Terms and Conditions (https://onlinelibrary.wiley.com/terms-and-conditions) on Wiley Online Library for rules of use; OA articles are governed by the applicable Creative Commons License

the number of bridging oxygens), centered at 65, 56 and 47 ppm, respectively,[30] thus confirming the silane partial condensation. The ^{1}H spectrum of P25@HD (Figure S4), supports the presence of uncondensed silanols, while the –OH resonance observed in P25 spectrum is only weakly present in the silanized sample.

TGA analysis and nitrogen physisorption experiments were performed to quantitatively assess the titania silanization and to determine the functionalization degree. The thermograms of naked P25 and P25_HT and of the corresponding P25@HD and P25_HT@HD functionalized NPs are reported in Figure S5. From the TGA curves and by considering the values of the specific surface area of the samples estimated by the BET method (see Figure S6 and Eqs. S1–S2, Section S3, Supporting Information) the grafting density of HDTMS for each modified sample and the hydroxylation degree for the P25 and P25_HT samples were calculated. The obtained figures are reported in Table 1, along with the values of the specific surface area.

According to these results, we can confirm that the hydrothermal treatment of P25 increases the surface hydroxylation, thus enhancing to some extent the grafting of HDTMS moieties onto the TiO_2 surface.[31]

HDTMS functionalization leads to the decrease of NPs SSA_{BET} values (Table 1). Therefore, contact angles were measured by means of the sessile drop method with deionized water to evaluate the surface wetting properties of titania nanoparticles before and after HDTMS grafting (Figure S7, Section S4, Supporting Information). As expected, the highly hydrophilic P25 surface (advancing contact angle: $24 \pm 7°$) turns to superhydrophobic after functionalization with HDTMS. As a matter of facts, P25_HT@HD displays advancing and receding contact angles higher than 150° and contact angle hysteresis of 1°.

Table 1: Specific surface area (SSA_{BET}) estimated by nitrogen physisorption, hydroxylation and functionalization degree calculated from TGA for naked and functionalized TiO_2 samples.

Samples	SSA_{BET} ($m^2 g^{-1}$)	σ (molecules nm^{-2})
P25	57.4 ± 0.3	7.99 (–OH)
P25_HT	52.09 ± 0.24	11.92 (–OH)
P25@HD	41.02 ± 0.28	2.50 (HDTMS)
P25_HT@HD	33.43 ± 0.21	2.71 (HDTMS)

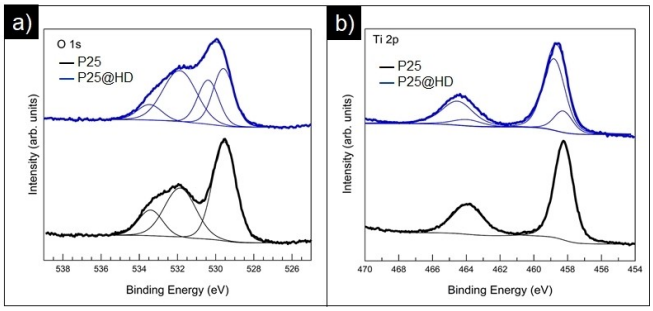

Figure 1. a) O *1s* and b) Ti *2p* XPS spectra of bare P25 (black line) and P25@HD (blue line) samples.

XPS survey was carried out to further study the surface features of both naked and silanized TiO_2 nanoparticles. In particular, O *1s* and Ti *2p* core levels recorded from P25 and P25@HD samples are shown in Figure 1.

The intense peaks at 529.5 eV and at ~532 eV in the O *1s* spectrum of P25 (Figure 1a) are due to O–Ti and Ti–O–H species, respectively.[32] A third component centered at 533.5 eV (Figure 1a), can be ascribed to adsorbed H_2O molecules.[33] The Ti $2p_{3/2}$ and Ti $2p_{1/2}$ components at around 458.2 eV and 464 eV (Figure 1b) in Ti *2p* region stand for the fingerprints of Ti–O bonds in TiO_2.[34,35] In the P25@HD sample the appearance of the Si *2p* peak at 102 eV (Figure S8, Supporting Information) in conjunction with the O *1s* component at 530.4 eV (Figure 1a), designated as Ti–O–Si, reveal the presence of the grafted silane moieties.[36,37] In P25@HD the increased broadness of signal at ~532 eV can be attributed to the presence of Si–O–H, in agreement with FTIR and NMR results (Figures S1 and S2b), as well as to residual Ti–O–H groups.[36,38] In addition, the decrease in intensity of adsorbed water peak at 533.5 eV (Figure 1a) is in agreement with the hydrophobicity of alkyl-modified TiO_2.[39]

Notably, a shift towards higher binding energy ($\Delta \sim +0.4$ eV) of the Ti *2p* peaks can be detected for the P25@HD sample (Figure 1b), confirming the generation of Si–O–Ti covalent bond.[35,40] In fact, the higher Si electronegativity (~1.9 eV) compared to that of Ti (~1.5 eV) may induce a partial decrease of the shielding effect of the valence electrons in Ti ions and, consequently, an increase of the BE of both the Ti *2p* components.[41] Similar XPS spectra have been retrieved for the P25_HT@HD sample. It is worth noting here that XPS analyses did not reveal the presence of Ti^{3+} in the investigated samples. By considering the extent of the surface modification and the long alkyl chains of the grafting moieties, it is reasonable to assume that the XPS results can be considered representative of outer surface, *i.e.* the first 1–2 atomic layers.

Adsorption/desorption experiments using both carbon monoxide and 2,6-dimethylpiridine (2,6-DMP) were carried out in order to evaluate changes in surface acidity after NPs functionalization. As a matter of facts, CO adsorption reveals the presence of Lewis acidic sites while 2,6-DMP is known to interact with both Lewis and Brønsted acidic sites. The details of the experiments are reported in Section S4, Supporting Information, and the FTIR spectra recorded on samples after exposure to different CO and 2,6-DMP pressure are shown in Figures S9 and S10, respectively. The comparison of the FTIR spectra recorded at the maximum CO pressure (100 torr) on P25 and P25@HD samples (Figure 2) clearly points out that surface functionalization prevents CO adsorption, contrarily to what observed in bare P25 that shows a signal at 2182 cm^{-1} due to the CO interaction with coordinatively unsaturated Ti^{4+} centers acting as Lewis acidic sites.[42] Adsorption/desorption tests performed on P25@HD sample with 2,6-DMP (Figure S10) confirm negligible Lewis acidity and reveal the presence of a very weak Brønsted acidity, which is not reported for TiO_2.[43,44]

© 2024 The Authors. Angewandte Chemie International Edition published by Wiley-VCH GmbH

15213773, 0, Downloaded from https://onlinelibrary.wiley.com/doi/10.1002/anie.202414445 by CochraneItalia, Wiley Online Library on [09/11/2024]. See the Terms and Conditions (https://onlinelibrary.wiley.com/terms-and-conditions) on Wiley Online Library for rules of use; OA articles are governed by the applicable Creative Commons License

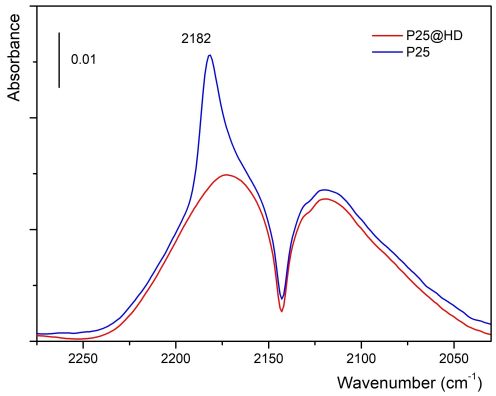

Figure 2. Comparison of the FTIR spectra recorded on P25 and P25@HD samples exposed to 100 Torr CO pressure.

EPR is a very sensitive tool for detecting paramagnetic defectivity induced upon processing or surface/bulk modification of metal oxides.[45] In detail, spectra were acquired at 130 K before and after UV irradiation *in vacuo* ($p < 10^{-5}$ mbar) (Figure 3a and b, respectively), and under UV irradiation in the presence of 20 mbar oxygen partial pressure (see Figure S11, Section S5, Supporting Information). Before UV irradiation, the spectra of naked titania samples showed the typical signal attributed by Gray *et al.*[46] to tetrahedrally distorted Ti^{3+} center in the interfacial region between rutile and anatase in P25 (Figure 3a), along with very weak signals at lower field probably connected to oxygen-related species (*i.e.* O^- and O_2^- centers). Interestingly, the surface silanization remarkably increases the intensity of these resonances, especially for the P25_HT@HD sample (shaded yellow area in Figure 3a). In accordance with the literature,[47] UV photoexcitation *in vacuo* (Figure 3b) of naked P25 and P25_HT leads to a broad and moderately intense signal related to different superimposed electron trap species (Ti^{3+} centers) and to weak features related to trapped holes (O^- species). The same experiment carried out on the functionalized samples gives rise to much more intense and defined Ti^{3+} resonances, along with overlapped signals at low magnetic field ascribable to different O^- and O_2^- species,[14,15] and, possibly, to E'($\equiv Si^{\cdot}$) defects.[48] This suggests that the surface functionalization of TiO_2 prevents the recombination of photogenerated electrons and holes by fostering their trapping into Ti^{3+} centers and in other lattice/surface defect centers, respectively. For naked titania, improved charge separation has been traditionally connected to enhanced interfacial charge transfer and, in turn, to remarkable photocatalytic properties.[49] However, in the present case, surface silanization suppresses the electron transfer to oxygen, as demonstrated recently by our studies and as reported in Figure S11, Supporting Information.[14,15] In fact, superoxide species could be detected for irradiated P25 in the presence of O_2 (spectrum 3 in Figure S11), in agreement with the literature,[50] but they were virtually absent in the silanized sample (spectrum 4 in Figure S11).

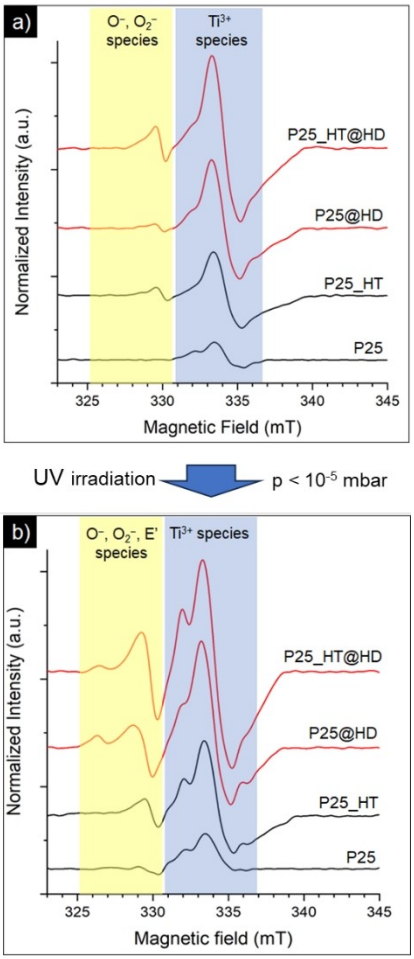

Figure 3. EPR spectra at 130 K *in vacuo* ($p < 10^{-5}$ mbar) of P25, P25_HT, P25@HD and P25_HT@HD samples a) before and b) after UV irradiation. Shaded areas are guides to discriminate the different paramagnetic species.

This indicates that, besides promoting charge trapping, surface functionalization effectively hampers the successive interfacial electron transfer to oxygen, significantly suppressing the generation of superoxide species.

From these results, the role played by Ti^{3+} centers emerges as essential, and it appears relevant to advance some hypotheses on the structural changes involving the titanium species upon TiO_2 silanization. In this perspective, and considering that the surface groups of functionalized titania can be assimilated to the Ti–O–Si≡ units at the interface of TiO_2/SiO_2 NPs, a survey of recent literature studies on similar TiO_2/SiO_2 systems can help to shed some light. Gao *et al.*[51] reported the existence of Ti^{3+} species in TiO_2/SiO_2 mixed oxides, attributed to the formation of oxygen vacancies at the interface between the oxides, with the two electrons remaining in the vacancy, moving toward the neighboring Ti atoms. Notably, in comparable materials, a change in the coordination field from octahedral to tetrahedral of titanium atoms at the interface with the silica counterpart has been additionally reported.[52,53] First principle calculations performed by Yin *et al.*[54] attributed the

© 2024 The Authors. Angewandte Chemie International Edition published by Wiley-VCH GmbH

15213773, 0, Downloaded from https://onlinelibrary.wiley.com/doi/10.1002/anie.202414445 by CochraneItalia, Wiley Online Library on [09/11/2024]. See the Terms and Conditions (https://onlinelibrary.wiley.com/terms-and-conditions) on Wiley Online Library for rules of use; OA articles are governed by the applicable Creative Commons License

generation of oxygen vacancies in TiO_2 to crystal field changes from octahedral to distorted tetrahedral coordination. Moreover, the authors showed that these oxygen vacancies are stabilized in the sub-surface region, where they can also cluster together.

According to these considerations, we may infer that P25 silanization induces changes in the crystal field of surface titanium atoms from octahedral to distorted tetrahedral coordination, which, in turn, stabilizes oxygen vacancies promoting the transfer of electrons to the Ti cation band structure, thus giving rise to Ti^{3+} centers in the sub-surface region. The increase of defective oxygen species upon silanization is witnessed by the increase of the corresponding EPR signals in Figure 3a (shaded yellow area). The location of Ti^{3+} species in the sub-surface region is in line with the missing evidence of these species in the first layers of the silanized samples revealed by XPS results and explains the inhibited interfacial electron transfer to oxygen in P25@HD sample (see EPR spectra in Section S5, Supporting Information).

The hypothesized higher amount of distorted titanium centers at the surface of the silanized samples compared to the naked ones could be corroborated by comparing the components of the diffuse reflectance spectra (DRS) of bare and silanized P25 samples in the UV region, as shown in Figure 4.

In detail, the UV absorption band of the samples has been deconvoluted into four gaussian components, which are the same as those proposed by Maheu *et al.*[55] for anatase and rutile phases. The components 1 (220–230 nm) and 3 (270–280 nm) are attributed to ligand-to-metal charge transfer from O^{2-} to Ti^{4+} in tetrahedral and octahedral coordination, respectively.[52,53] The ratio between these components indicates that the number of Ti atoms tetrahedrally coordinated increases upon silanization. Similar results have been obtained for the P25_HT and P25_HT@HD samples (Figure S12, Section S6 Supporting Information).

Singlet Oxygen Generation and Photocatalytic Activity

Singlet Oxygen Sensor Green (SOSG) is a selective sensor used for $^1O_2$ detection. This molecule combines a chromophore part and an electron donor fragment, quenching the fluorescence of the chromophore as a result of intramolecular electron transfer. The electron donor can be oxidized by $^1O_2$ to the corresponding endoperoxide product, which is unable to quench the fluorescence of the chromophore. Therefore, the emission of SOSG is evident upon its oxidation with singlet oxygen (Figure 5, bottom).[56]

Results show that the $^1O_2$ generation is remarkably dependent on the surface functionalization. In fact, while pure P25 and P25_HT NPs display just a trivial increase in the singlet oxygen generation, a marked sensitization effect can be noticed for both functionalized samples (Figure 5, top).

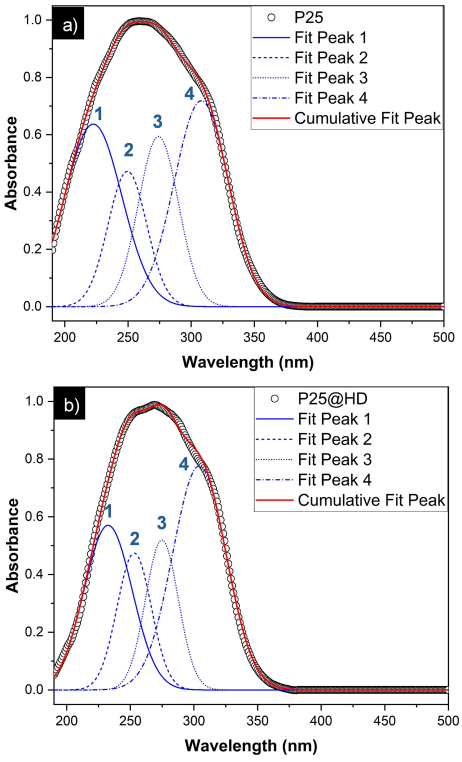

Figure 4. Normalized and deconvoluted UV/Vis absorbance spectra of a) P25 and b) P25@HD samples.

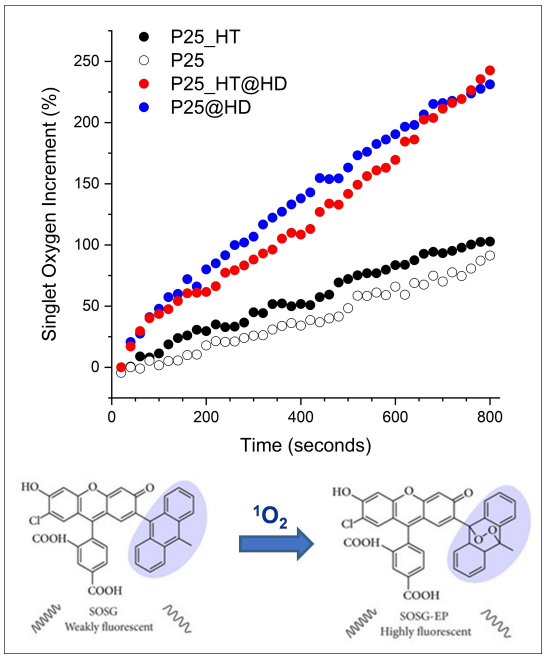

Figure 5. Top: $^1O_2$ evolution calculated from the increment in emission intensity measured after 20–800 sec of simultaneous excitation with soft X-rays and optical light at 473 nm, and directly after the addition to the solutions of SOGS (*i.e.* t = 0 sec) in the presence of bare P25 and P25_HT (black hollow and full circles, respectively) and of P25@HD (blue circles) and P25_HT@HD (red circles). Bottom: Scheme of SOGS oxidation by $^1O_2$ to produce the corresponding endoperoxide product (SOSG-EP).

© 2024 The Authors. Angewandte Chemie International Edition published by Wiley-VCH GmbH

15213773, 0, Downloaded from https://onlinelibrary.wiley.com/doi/10.1002/anie.202414445 by CochraneItalia, Wiley Online Library on [09/11/2024]. See the Terms and Conditions (https://onlinelibrary.wiley.com/terms-and-conditions) on Wiley Online Library for rules of use; OA articles are governed by the applicable Creative Commons License

It is worth noting that the observed weak Brønsted acidity and hydrophobicity of the silanized sample did not significantly affect the dark adsorption of molecular oxygen (see Figure S13, Section S7, Supporting Information, for experimental details).[57] Therefore, the increased production of singlet oxygen cannot be attributed to trivial surface excess effects, as previously proposed for similar systems.[58]

In order to further highlight the enhanced formation of singlet oxygen upon TiO_2 silanization, we performed the photocatalytic epoxidation of limonene to 1,2 limonene epoxide (Scheme 2), as a model reaction triggered by singlet oxygen through a Schenck-ene mechanism.[12] Reactions have been performed under air atmosphere. Results of tests in the presence of nitrogen or oxygen atmosphere are reported in Figure S14, Section S8, Supporting Information. Conversion and selectivity values have been calculated according to Eqs. S3 and S4, respectively.

Figure 6 shows the values of limonene conversion and selectivity towards the epoxide during a representative run under UV irradiation in the presence of P25_HT and P25_HT@HD samples.

Titania silanization significantly suppresses the conversion of limonene, while the selectivity towards the epoxide experiences a twofold increase. The lower limonene conversion can be justified by considering the lower efficiency of the interfacial electron transfer revealed by EPR analysis. On the other hand, selectivity results can be correlated with both the higher amount of singlet oxygen detected in the presence of the silanized sample and the stabilization of Ti^{3+} centers, whose concentration increases upon silanization. The suppressed electron transfer observed by EPR spectroscopy makes unlikely Dexter-type energy transfer mechanisms, *i.e.* based on sequential or concerted double electron transfer in opposite directions. However, long range dipole-dipole interactions, such as Förster-type energy transfer involving the excited Ti^{3+} species as the energy donor and the molecular oxygen as the energy acceptor, seem more plausible. In fact, orbital overlapping is not required for this type of energy transfer mechanism, and the distance between the Ti^{3+} centers in the sub-surface region and the oxygen adsorbed at the surface is comparable with the Förster distance.[59]

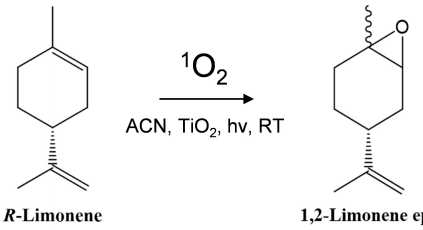

Scheme 2. Photocatalytic *R*-limonene epoxidation to 1,2-limonene epoxide.

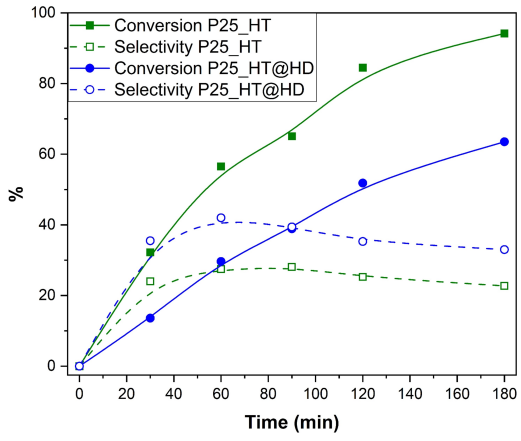

Figure 6. Limonene conversion (%, full symbols) and selectivity towards the corresponding epoxide (%, empty symbols) during a representative run under UV irradiation in the presence of P25_HT (green symbols) and P25_HT@HD (blue symbols) samples. Selected runs have been performed in triplicate with a deviation of ±3%.

Notably, the maximum absorbance wavelength of Ti^{3+} is reported to be 780 nm.[22] Therefore, NIR irradiation should be capable of boosting the energy transfer from these sub-surface defects to oxygen, thus increasing the production of singlet oxygen. To check this hypothesis, we performed the photocatalytic limonene epoxidation in the presence of bare and silanized P25 samples, under UV light and simultaneous UV and NIR irradiation, as shown in Figure 7. Notably, no reactivity was observed under visible or sole NIR irradiation, both in the presence or in the absence of the photocatalyst, suggesting that trivial excitation can be probably excluded and that an effective population of the sub-surface Ti^{3+} states is required. Results in the presence of bare and silanized P25_HT are comparable.

The limonene conversion is not affected by the use of NIR irradiation in the presence of bare P25 (Figure 7, top Panel, full symbols). Instead, it is higher if NIR radiation is additionally used in the presence of the silanized sample (Figure 7, bottom Panel, full symbols). This suggests that the influence of NIR irradiation is negligible when electron transfer is the prevailing primary event, as in the case of bare TiO_2, but becomes relevant when energy transfer mechanisms are preferentially taking place. In fact, the formation of OH radicals is very low using acetonitrile as the solvent,[60] and the formation of superoxide is quenched by the surface silanization, as demonstrated by EPR spectroscopy. Conversely, the selectivity values towards the epoxide are always higher under simultaneous NIR irradiation for both bare and silanized samples. This further confirms the role of sub-surface Ti^{3+} centers acting as NIR excitable photosensitizers for singlet oxygen formation.

The photocatalytic results obtained in the presence of limonene could be qualitatively reproduced also for other olefins of different nature such as styrene, 1-octene, 4-octene, and cyclohexene. In fact, in all of the cases the selectivity values towards the corresponding epoxide almost doubled when using the silanized sample instead of the bare one. Moreover, simultaneous NIR irradiation triggered further selectivity increment (up to 10%), similarly to what reported for the case of limonene. Results are shown in Figure S15 and summarized in Table S2, Section S9, Supporting Information.

© 2024 The Authors. Angewandte Chemie International Edition published by Wiley-VCH GmbH

15213773, 0, Downloaded from https://onlinelibrary.wiley.com/doi/10.1002/anie.202414445 by Cochraneltalia, Wiley Online Library on [09/11/2024]. See the Terms and Conditions (https://onlinelibrary.wiley.com/terms-and-conditions) on Wiley Online Library for rules of use; OA articles are governed by the applicable Creative Commons License

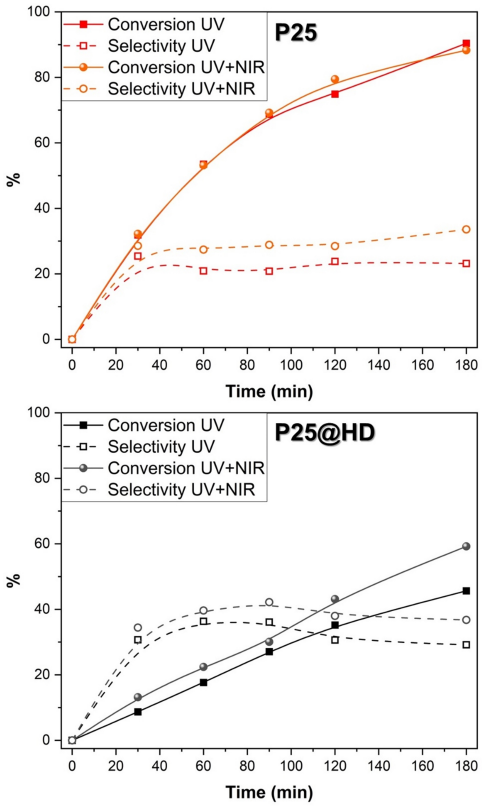

Figure 7. Limonene conversion (%, full symbols) and selectivity towards the epoxide (%, empty symbols) during representative runs under UV (squares) and simultaneous UV and NIR irradiation (circles) in the presence of P25 (top Panel) and P25@HD (bottom Panel) samples. Selected runs have been performed in triplicate with a deviation of ±3%.

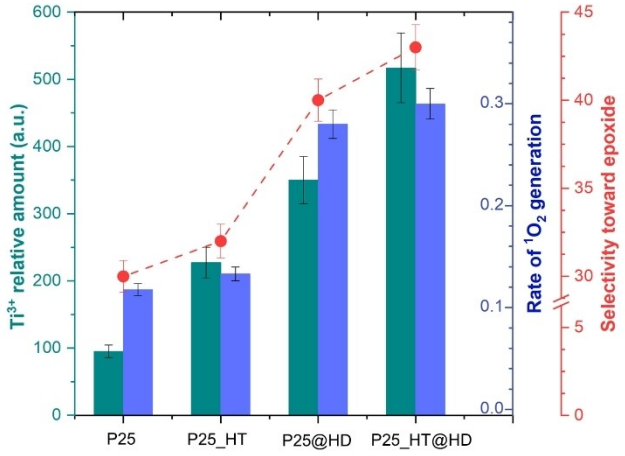

Figure 8. Semi-quantitative correlation among Ti^{3+} relative amount (green bars) detected by EPR, rate of singlet oxygen generation from SOSG experiments (blue bars), and highest selectivity values towards 1,2 limonene epoxide (red circles) obtained in the photocatalytic partial oxidation of limonene for P25, P25_HT, P25@HD, and P25_HT@HD samples.

Finally, Figure 8 summarizes semi-quantitatively the discussed correlations among the Ti^{3+}relative amount detected by EPR spectroscopy (derived from double integration of Ti^{3+} resonance lines intensity), the singlet oxygen generation rate (*i.e.* the initial slope in the curve of $^1O_2$ increment vs. time), and the highest selectivity values towards 1,2 limonene epoxide obtained in the presence of the selected TiO_2 samples. All of the three parameters, measured through independent tests, increase consistently by increasing the silanization degree of the surface, indicating the role of sub-surface Ti^{3+} centers, stabilized upon silanization, in the photocatalytic generation of singlet oxygen.

Conclusions

Modification of the surface of TiO_2 NPs with a long-chain alkyl silane induces structural and opto-electronic changes, which eventually affect the nature and distribution of the photocatalytically generated reactive oxygen species. In particular, silanization induces a decrease of the electronic density around the surface Ti centers directly linked to the grafting moiety, and a local change of their coordination environment, which results in the stabilization of Ti^{3+} centers in the sub-surface region. The electron transfer from these sub-surface Ti^{3+} centers to molecular oxygen adsorbed at the surface is hindered, as revealed by the suppressed formation of superoxide radical species. On the other hand, the rate of formation of singlet oxygen increases by increasing the relative amount of Ti^{3+} centers, which could act as NIR-absorbing oxygen photosensitizers. Accordingly, the partial oxidation of several olefins to the corresponding epoxides occurs with improved selectivity in the presence of higher amount of Ti^{3+} centers and under simultaneous UV and NIR irradiation. Results indicate that the generation of singlet oxygen in silanized TiO_2 samples occurs mainly through Förster-type energy transfer mechanism.

Supporting Information

The authors have cited additional references within the Supporting Information.[61–63]

Acknowledgements

The authors wish to thank Prof. G. Cerrato (University of Torino) for the surface acidity tests and Prof. V. Vaiano (University of Salerno) for the oxygen adsorption tests. Open Access publishing facilitated by Università degli Studi di Trento, as part of the Wiley - CRUI-CARE agreement.

Conflict of Interest

The authors declare no conflict of interest.

© 2024 The Authors. Angewandte Chemie International Edition published by Wiley-VCH GmbH

15213773, 0, Downloaded from https://onlinelibrary.wiley.com/doi/10.1002/anie.202414445 by CochraneItalia, Wiley Online Library on [09/11/2024]. See the Terms and Conditions (https://onlinelibrary.wiley.com/terms-and-conditions) on Wiley Online Library for rules of use; OA articles are governed by the applicable Creative Commons License

Data Availability Statement

The data that support the findings of this study are available from the corresponding author upon reasonable request.

Keywords: Energy transfer · Limonene · Photocatalysis · Silanized TiO_2 · Singlet oxygen

[1] O. U. Akakuru, Z. M. Iqbal, A. Wu, in *TiO_2 Nanoparticles*, **2020**, pp. 1–66.
[2] D. B. Warheit, S. C. Brown, *Toxicol. Lett.* **2019**, *302*, 42; C.-C. Li, S.-J. Chang, M.-Y. Tai, *J. Am. Ceram. Soc.* **2010**, *93*, 4008.
[3] B. Dréno, A. Alexis, B. Chuberre, M. Marinovich, *J. Eur. Acad. Dermatol. Venereol.* **2019**, *33*, 34.
[4] A. K. M. Fung, B. K. W. Chiu, M. H. W. Lam, *Water Res.* **2013**, *37*, 1939.
[5] a) M. R. Ataabadi, M. Jamshidi, *Sci. Rep.* **2023**, *13*, 7383; b) F. S. Gul, A. Bahader, M. Nawaz, S. Zahmatkesh, S. Iikela, K. T. T. Amesho, *Environ. Monit. Assess.* **2023**, *195*, 777; c) X. Yan, T. Ohno, K. Nishijima, R. Abe, B. Ohtani, *Chem. Phys. Lett.* **2006**, *429*, 606.
[6] F. Parrino, C. De Pasquale, L. Palmisano, *ChemSusChem* **2019**, *12*, 589.
[7] a) K. Inumaru, T. Kasahara, M. Yasui, S. Yamanaka, *Chem. Commun.* **2005**, 2131; b) K. Inumaru, M. Yasui, T. Kasahara, K. Yamaguchi, A. Yasuda, S. Yamanaka, *J. Mater. Chem.* **2011**, *21*, 12117.
[8] Y. Shiraishi, Y. Sugano, D. Inoue, T. Hirai, *J. Catal.* **2009**, *264*, 175.
[9] A. R. Almeida, J. T. Carneiro, J. A. Moulijn, G. Mul, *J. Catal.* **2010**, *273*, 116.
[10] F. Parrino, A. Di Paola, V. Loddo, I. Pibiri, M. Bellardita, L. Palmisano, *Appl. Catal. B* **2016**, *182*, 347.
[11] A. Jańczyk, E. Krakowska, G. Stochel, W. Macyk, *J. Am. Chem. Soc.* **2006**, *128*, 15574.
[12] R. Ciriminna, F. Parrino, C. De Pasquale, L. Palmisano, M. Pagliaro, *Chem. Commun.* **2018**, *54*, 1008.
[13] A. Gottuso, A. Köckritz, M. L. Saladino, F. Armetta, C. De Pasquale, G. Nasillo, F. Parrino, *J. Catal.* **2020**, *391*, 202.
[14] F. Parrino, M. D'Arienzo, E. Callone, R. Conta, B. Di Credico, S. Mascotto, A. Meyer, R. Scotti, S. Dirè, *Chem. Eng. J.* **2021**, *417*, 129135.
[15] F. Parrino, M. D'Arienzo, S. Mostoni, S. Dirè, R. Ceccato, M. Bellardita, L. Palmisano, *Top. Curr. Chem.* **2022**, *380*.
[16] V. M. Kiselev, I. M. Kislyakov, A. N. Burchinov, *Opt. Spectrosc.* **2016**, *120*, 520.
[17] A. V. Demyanenko, A. S. Bogomolov, N. V. Dozmorov, A. I. Svyatova, A. P. Pyryaeva, V. G. Goldort, S. A. Kochubei, A. V. Baklanov, *J. Phys. Chem. C* **2019**, *123*, 28515.
[18] N. J. Turro, *Pure Appl. Chem.* **1977**, *49*, 405.
[19] T. Daimon, Y. Nosaka, *J. Phys. Chem. C* **2007**, *111*, 4420.
[20] Y. Nosaka, T. Daimon, A. Y. Nosaka, Y. Murakami, *Phys. Chem. Chem. Phys.* **2004**, *6*, 2917.
[21] T. Förster, *Ann. Phys.* **1948**, *437*, 55.
[22] M. Buchalska, P. Łabuz, Ł. Bujak, G. Szewczyk, T. Sarna, S. Maćkowski, W. Macyk, *Dalton Trans.* **2013**, *42*, 9468.
[23] J. Yu, H. Yu, B. Cheng, M. Zhou, X. Zhao, *J. Mol. Catal. A* **2006**, *253*, 112.
[24] a) A. Moral, F. Borrull, K. G. Furton, A. Kabir, N. Fontanals, R. M. Marcé, *J. Chromatogr. A* **2022**, *1676*, 463237; b) G. Socrates, *Infrared and Raman characteristic group frequencies: Tables and charts, 3rd Edition*, John Wiley & Sons Ltd, England, **2004**.
[25] P. Launer, B. Arkles, in *Silicon Compounds: Silanes & Silicones*, **2013**, pp. 175.
[26] a) S. P. Pujari, L. Scheres, A. T. M. Marcelis, H. Zuilhof, *Angew. Chem. Int. Ed.* **2014**, *53*, 6322; b) R. M. Almeida, A. C. Marques, in *Handbook of Sol-Gel Science and Technology* (Eds.: L. Klein, M. Aparicio, A. Jitianu), Springer, Cham, **2016**, pp. 1–31; c) B. Indumathy, P. Sathiyanathan, G. Prasad, M. S. Reza, A. A. Prabu, H. Kim, *Polymer* **2023**, *15*, 2517.
[27] Y. Wang, H. Li, X. Liu, C. Yu, *J. Wood Chem. Technol.* **2021**, *41*, 25.
[28] J. Cheng, M. Fone, M. W. Ellsworth, *Solid State Nucl. Magn. Reson.* **1996**, *7*, 135.
[29] H. O. Fatunmbi, M. D. Bruch, *Langmuir* **2013**, *29*(16), 4974.
[30] P. Mingarelli, C. Romeo, E. Callone, G. Fredi, A. Dorigato, M. D'Arienzo, F. Parrino, S. Dirè, *Gels* **2023**, *9*, 810.
[31] A. A. Issa, A. S. Luyt, *Polymer* **2019**, *11*, 537.
[32] W.-H. Liao, S.-T. Hsiao, Y.-F. Wu, S.-J. Zeng, S.-M. Li, Y.-S. Wang, C.-C. M. Ma, *RSC Adv.* **2014**, *4*, 38614.
[33] S. Benkoula, O. Sublemontier, M. Patanen, C. Nicolas, F. Sirotti, A. Naitabdi, F. Gaie-Levrel, E. Antonsson, D. Aureau, F.-X. Ouf, S.-I. Wada, A. Etcheberry, K. Ueda, C. Miron, *Sci. Rep.* **2015**, *5*, 15088.
[34] B. Erdem, R. A. Hunsicker, G. W. Simmons, E. D. Sudol, V. L. Dimonie, M. S. El-Aasser, *Langmuir* **2001**, *17*, 2664.
[35] G. Y. Song, I. Jang, S.-W. Jeon, S.-H. Ahn, J.-Y. Kim, S. y. Kim, G. Sa, *J. Ind. Eng. Chem.* **2021**, *94*, 180.
[36] N. Paengjun, K. Vibulyaseak, M. Ogawa, *Sci. Rep.* **2021**, *11*, 3210.
[37] G. M. Ingo, S. Dirè, F. Babonneau, *Appl. Surf. Sci.* **1993**, *70–71*, 230.
[38] E. Paparazzo, M. Fanfoni, E. Severini, S. Priori, *J. Vac. Sci. Technol. A* **1992**, *10*, 2892.
[39] J. Guo, S. Yuan, Y. Yu, J. R. van Ommen, H. Van Bui, B. Liang, *RSC Adv.* **2017**, *7*, 4547.
[40] I. Jang, J.-H. Park, K. Song, S. Kim, Y. Lee, S.-G. Oh, *Mater. Chem. Phys.* **2014**, *147*, 691.
[41] L. Yuan, C. Han, M. Pagliaro, Y.-J. Xu, *J. Phys. Chem. C* **2016**, *120*, 265.
[42] M. Minella, M. G. Faga, V. Maurino, C. Minero, E. Pelizzetti, S. Coluccia, G. Martra, *Langmuir* **2010**, *26*, 2521–2527.
[43] L. Ferretto, A. Glisenti, *Chem. Mater.* **2003**, *15*, 1181–1188.
[44] V. Lebarbier, G. Clet, M. Houalla, *J. Phys. Chem. B* **2006**, *110*, 22608–22617.
[45] M. Chiesa, E. Giamello, M. Che, *Chem. Rev.* **2010**, *110*, 1320.
[46] D. C. Hurum, A. G. Agrios, K. A. Gray, T. Rajh, M. C. Thurnauer, *J. Phys. Chem. B* **2003**, *107*, 4545.
[47] a) S.-C. Ke, T.-C. Wang, M.-S. Wong, N. O. Gopal, *J. Phys. Chem. B* **2006**, *110*, 11628; b) D. C. Hurum, K. A. Gray, T. Rajh, M. C. Thurnauer, *J. Phys. Chem. B* **2005**, *109*, 977; c) M. Anpo, T. Shima, T. Fujii, S. Suzuki, M. Che, *Chem. Lett.* **1987**, *16*, 1997; d) D. C. Hurum, A. G. Agrios, S. E. Crist, K. A. Gray, T. Rajh, M. C. Thurnauer, *J. Electron Spectrosc. Relat. Phenom.* **2006**, *150*, 155.
[48] a) E. Richards, D. M. Murphy, M. Che, *Res. Chem. Intermed.* **2019**, *45*, 5763; b) W. H. Saputera, H. A. Tahini, M. Sabsabi, T. H. Tan, N. M. Bedford, E. Lovell, Y. Cui, J. N. Hart, D. Friedmann, S. C. Smith, R. Amal, J. Scott, *ACS Catal.* **2019**, *9*, 2674; c) M. D'Arienzo, J. Carbajo, A. Bahamonde, M. Crippa, S. Polizzi, R. Scotti, L. Wahba, F. Morazzoni, *J. Am. Chem. Soc.* **2011**, *133*, 17652.
[49] a) M. D'Arienzo, M. V. Dozzi, M. Redaelli, B. D. Credico, F. Morazzoni, R. Scotti, S. Polizzi, *J. Phys. Chem. C* **2015**, *119*, 12385; b) A. Testino, I. R. Bellobono, V. Buscaglia, C. Canevali, M. D'Arienzo, S. Polizzi, R. Scotti, F. Morazzoni, *J. Am. Chem. Soc.* **2007**, *129*, 3564; c) R. Chen, F. Fan, C. Li, *Angew. Chem. Int. Ed.* **2022**, *61*, e202117567; d) R. Yanagi, T. Zhao, D. Solanki, Z. Pan, S. Hu, *ACS Energy Lett.* **2022**, *7*, 432.

© 2024 The Authors. Angewandte Chemie International Edition published by Wiley-VCH GmbH

15213773, 0, Downloaded from https://onlinelibrary.wiley.com/doi/10.1002/anie.202414445 by Cochraneltalia, Wiley Online Library on [09/11/2024]. See the Terms and Conditions (https://onlinelibrary.wiley.com/terms-and-conditions) on Wiley Online Library for rules of use; OA articles are governed by the applicable Creative Commons License

[50] a) A. L. Attwood, D. M. Murphy, J. L. Edwards, T. A. Egerton, R. W. Harrison, *Res. Chem. Intermed.* **2003**, *29*, 449; b) E. Carter, A. F. Carley, D. M. Murphy, *J. Phys. Chem. C* **2007**, *111*, 10630.
[51] X. Gao, S. R. Bare, J. L. G. Fierro, M. A. Banares, I. E. Wachs, *J. Phys. Chem. B* **1998**, *102*, 5653.
[52] S. Budhi, C.-M. Wu, D. Zhao, R. T. Koodali, in *Catalysts, Vol. 5*, **2015**, 1603.
[53] R. Peng, D. Zhao, N. M. Dimitrijevic, T. Rajh, R. T. Koodali, *J. Phys. Chem. C* **2012**, *116*, 1605.
[54] W. Yin, B. Wen, Q. Ge, X. Wei, G. Teobaldi, L. Liu, *Prog. Nat. Sci.* **2020**, *30*, 128.
[55] C. Maheu, L. Cardenas, E. Puzenat, P. Afanasiev, C. Geantet, *Phys. Chem. Chem. Phys.* **2018**, *20*, 25629.
[56] a) É. Hideg, *Cent. Eur. J. Biol.* **2008**, *3*, 273; b) A. Gollmer, J. Arnbjerg, F. H. Blaikie, B. W. Pedersen, T. Breitenbach, K. Daasbjerg, M. Glasius, P. R. Ogilby, *Photochem. Photobiol.* **2011**, *87*, 671; c) S. Kim, M. Fujitsuka, T. Majima, *J. Phys. Chem. B* **2013**, *117*, 13985.
[57] L. Liu, P. Crawford, P. Hu, *Prog. Surf. Sci.* **2009**, *84*, 155–176.
[58] X. Chen, X. Sheng, H. Zhou, Z. Liu, M. Xu, X. Feng, *Small* **2024**, *20*, 2310128.
[59] K. E. Sapsford, L. Berti, I. L. Medintz, *Angew. Chem. Int. Ed.* **2006**, *45*, 4562.
[60] a) A. Gottuso, C. De Pasquale, S. Livraghi, L. Palmisano, S. Diré, R. Ceccato, F. Parrino, *J. Mol. Catal.* **2023**, *550*, 113607; b) N. Morante, A. Gottuso, F. Parrino, V. Vaiano, *Catal. Today* **2024**, *432*, 114600.
[61] L. Zhu, Q. Gu, P. Sun, W. Chen, X. Wang, G. Xue, *ACS Appl. Mater. Interfaces* **2013**, *5*, 10352.
[62] C. Morterra, *J. Chem. Soc. Faraday Trans. 1* **1988**, *84*, 1617–1637.
[63] C. Morterra, G. Cerrato, *Langmuir* **2001**, *17*, 7053–7060.

Manuscript received: July 30, 2024
Accepted manuscript online: October 4, 2024
Version of record online: ■■, ■■

© 2024 The Authors. Angewandte Chemie International Edition published by Wiley-VCH GmbH

15213773, 0, Downloaded from https://onlinelibrary.wiley.com/doi/10.1002/anie.202414445 by CochraneItalia, Wiley Online Library on [09/11/2024]. See the Terms and Conditions (https://onlinelibrary.wiley.com/terms-and-conditions) on Wiley Online Library for rules of use; OA articles are governed by the applicable Creative Commons License

Research Article

Photocatalysis

F. Parrino,* A. Gottuso, L. Viganò, P. Mariani, I. Villa, F. Cova, E. Callone, S. Dirè, L. Palmisano, M. Stredansky, M. D'Arienzo **e202414445**

Singlet Oxygen Photocatalytic Generation by Silanized TiO_2 Nanoparticles

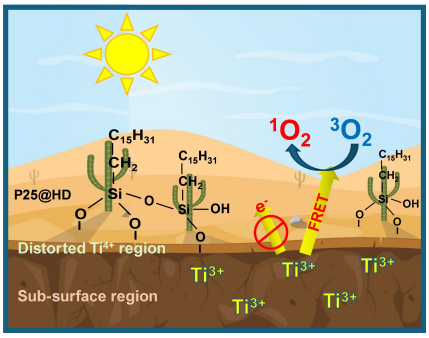

Surface silanization of TiO_2 (P25) with hexadecylsilane (HD) induces changes in the coordination of surface titanium centers and stabilizes Ti^{3+} defects in the sub-surface region. These defects could act as photosensitizers for the production of singlet oxygen through Förster-type resonance energy transfer (FRET), while interfacial electron transfer is efficiently suppressed.

© 2024 The Authors. Angewandte Chemie International Edition published by Wiley-VCH GmbH

15213773, 0, Downloaded from https://onlinelibrary.wiley.com/doi/10.1002/anie.202414445 by CochraneItalia, Wiley Online Library on [09/11/2024]. See the Terms and Conditions (https://onlinelibrary.wiley.com/terms-and-conditions) on Wiley Online Library for rules of use; OA articles are governed by the applicable Creative Commons License